ADVANCED MATERIALS TECHNOLOGIES
www.advmattechnol.de

Active Membranes on Rigidity Tunable Foundations for Programmable, Rapidly Switchable Adhesion

*Matthew D. Swift, Cole B. Haverkamp, Christopher J. Stabile, Dohgyu Hwang, Raymond H. Plaut, Kevin T. Turner, David A. Dillard, and Michael D. Bartlett**

Rapidly controlling and switching adhesion is necessary for applications in robotic gripping and locomotion, pick and place operations, and transfer printing. However, switchable adhesives often display a binary response (on or off) with a narrow adhesion range, lack post-fabrication adhesion tunability, or switch slowly due to diffusion-controlled processes. Here, pneumatically controlled shape and rigidity tuning is coupled to rapidly switch adhesion (≈0.1 s) across a wide range of programmable adhesion forces with measured switching ratios as high as 1300*x*. The switchable adhesion system introduces an active polydimethylsiloxane membrane supported on a compliant, foam foundation with pressure-tunable rigidity where positive and negative pneumatic pressure synergistically control contact stiffness and geometry to activate and release adhesion. Energy-based modeling and finite element computation demonstrate that high adhesion is achieved through a pressure-dependent, nonlinear stiffness of the foundation, while an inflated shape at positive pressures enables easy release. This approach enables adhesion-based gripping and material assembly, which is utilized to pick-and-release common objects, rough and porous materials, and arrays of elements with a greater than 14 000*x* range in mass. The robust assembly of diverse components (rigid, soft, flexible) is then demonstrated to create a soft and stretchable electronic device.

Switchable adhesives can rapidly and reversibly switch between a high and low adhesive state.[1] Such materials are critical for the development of reliable attachment with controlled release for applications ranging from robotic gripping and locomotion to transfer printing and assembly.[2–5] Switchable adhesives are typically achieved through a variety of triggers including thermal activation,[6–8] fluidic/solvent swelling,[9–11] electromagnetic actuation,[12–14] and mechanically based triggers.[15–19] A key performance metric is the adhesive switching ratio, $SR \equiv F_{high}/F_{low}$, where F_{high} is the adhesive force in the "on" state and F_{low} is the adhesive force in the "off" state. Furthermore, the switching time is the time required to switch from a high to low adhesive state. Rigidity or shape change at interfaces can enable adhesion switching through high compliance during contact and release, and increased rigidity during loading to achieve high loads through the minimization of strain energy.[20,21] Phase-change materials present a strategy to control the rigidity of an interface to switch adhesion. However, rapid switching at larger length scales can be challenging with processes that rely on diffusion, where heat or mass transfer can limit switching times to the order of 10 s or 100 s.[21–23] Furthermore, phase-change systems typically display a binary adhesion response, limiting adhesion tunability within a single system. To date, the ability to control and rapidly generate a wide range of adhesion forces remains a significant challenge.

Mechanical triggers have the potential to achieve rapid switching times and high switching ratios across length scales. This can include controlled loading trajectories through directional microstructured adhesives and reversible film adhesives.[24–26] Additionally, pneumatic systems that utilize adhesion can go beyond traditional vacuum grippers, as vacuum grippers can struggle with porous, irregular, or multiple discrete objects. For example, changing the shape of an interface with pneumatically inflatable membranes can reduce adhesion through the change in shape at the interface, which drives delamination and has demonstrated switching ratios of up to 50*x* with switching times on the order of seconds.[27,28] Membranes can also be actuated with additional stimuli, which can

M. D. Swift, C. B. Haverkamp, D. Hwang,[+] M. D. Barlett[+]
Materials Science & Engineering
Iowa State University
Ames, IA 50011, USA
E-mail: mbartlett@vt.edu
C. J. Stabile, K. T. Turner
Department of Mechanical Engineering and Applied Mechanics
University of Pennsylvania
Philadelphia, PA 19104, USA
R. H. Plaut
Department of Civil and Environmental Engineering
Virginia Tech
Blacksburg, VA 24061, USA
D. A. Dillard
Department of Biomedical Engineering and Mechanics
Virginia Tech
Blacksburg, VA 24061, USA
The ORCID identification number(s) for the author(s) of this article can be found under https://doi.org/10.1002/admt.202000676.
[+]Present address: Department of Mechanical Engineering, Soft Materials and Structures Lab, Virginia Tech, Blacksburg, VA 24061, USA

DOI: 10.1002/admt.202000676

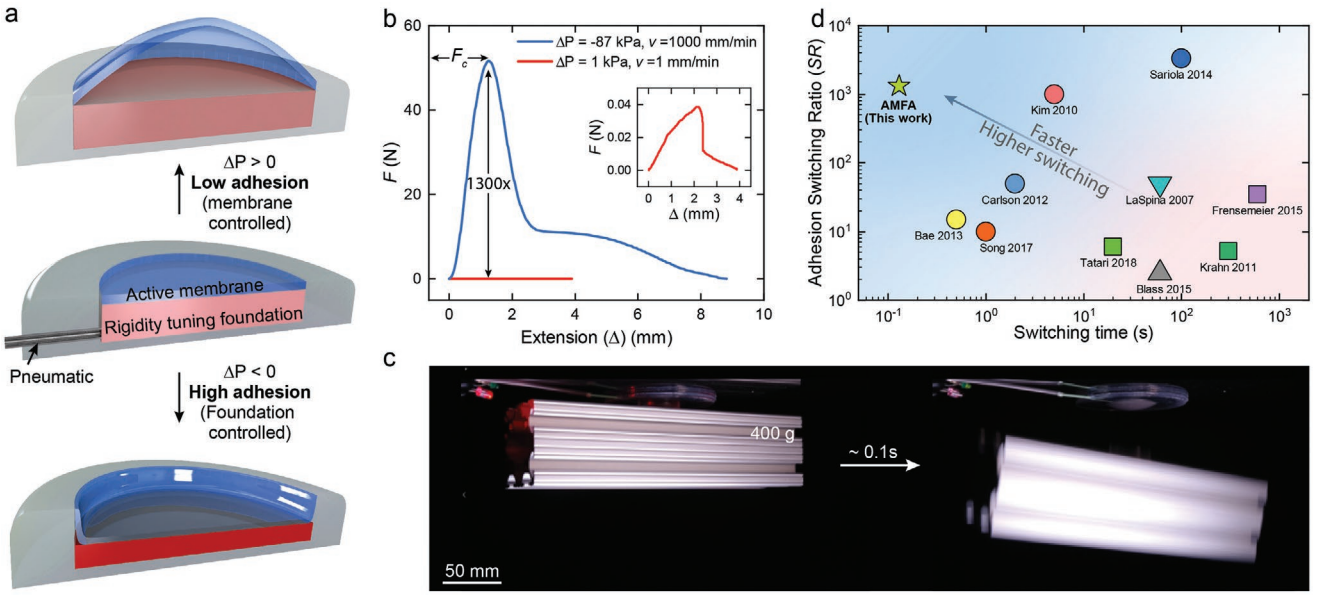

Figure 1. Rapidly switchable adhesives through active membrane-foundation adhesives (AMFAs). a) Schematic of an AMFA in the low adhesion and high adhesion states. b) Representative force versus extension data showing the high switching ratio when coupling pressure control with velocity control ($R = 15$ mm, smooth acrylic indenter); inset is for $\Delta P = 1$ kPa. c) Adhesive holding and then rapidly releasing a 400 g aluminum bar. d) Adhesion Switching Ratio (SR) versus switching time shows that AMFAs occupy a unique region of the switchable adhesion space. Data point shape represents switching triggers: ○ = mechanical, □ = thermal, △ = electricity/magnetism/light, ∇ = fluid.

include laser driven thermal switching of surfaces[29] as well as magnetically actuated membranes,[30] which can be used to print onto diverse surfaces or at programmed locations. Furthermore, negative pressure applied to membranes coated with micropillars can enhance load sharing to improve adhesion to diverse substrates.[31] However, adhesion switching ratios for these systems are on the order of 10, showing that pneumatic pressure alone cannot provide dramatic switching ratios as seen in phase-change materials. Microstructured soft robotic grippers can also improve adhesion through system-wide shape change with controlled interfacial structures.[32] These mechanisms, which control the shape of an interface, offer opportunities to achieve switchable adhesion with multiple adherence states through control of applied pneumatic pressure. However, systematically coupling rapid shape and rigidity tuning at interfaces to achieve multiple switchable adhesive states has not been demonstrated.

Here, we utilize a pneumatically controlled active polydimethylsiloxane (PDMS) membrane supported on a rigidity tunable foam foundation to rapidly switch adhesion through the systematic control of interfacial stiffness and contact geometry (**Figure 1**a). By coupling the membrane with a foam foundation that has pressure-tunable stiffness, these active membrane-foundation adhesives (AMFAs) leverage both positive and negative applied gauge pressures to enable a spectrum of programmable adhesion not previously demonstrated. When applying a positive pressure ($\Delta P > 0$), the membrane inflates and adhesion is reduced. When applying a negative pressure ($\Delta P < 0$), the foam compresses, dynamically adjusting stiffness and resulting in a rapid and dramatic increase in adhesion. We also show that separation velocity (v) can be utilized to further enhance adhesion response. Through these mechanisms, we find that adhesion can be switched on the order of 0.1 s with adhesion switching ratios as high as 1300x (Figure 1b,c). This combination of switching time and switching ratio is unique across a variety of switchable adhesive systems (Figure 1d). This exceptional combination is enabled by the foam foundation, which pneumatically changes stiffness orders of magnitude faster than diffusion-based processes that rely on thermal or solvent transport, coupled with the adhesive membrane, which can dramatically change interfacial shape through both positive and negative pneumatic pressure. Further, the elastic membrane allows for high reversibility where performance is maintained for at least 100 cycles with no sign of deterioration (Figure S1, Supporting Information). Analytical and numerical modeling finds good agreement with experimental data, providing design parameters to control adhesion response through pneumatic pressure and contact geometry, and highlighting the role of foundation rigidity on membrane adhesion. We demonstrate the precise and robust control of adhesion by utilizing an active membrane to pick-and-release common objects, porous materials, and arrays of elements and assemble dissimilar materials such as flex circuits and rigid LEDs to create soft and stretchable electronics.

The adhesive consists of a deformable membrane supported on a porous, compliant foundation (foam). The soft, foam foundation enables: i) intimate contact between the membrane and the target substrate/object, ii) communicates air quickly to provide positive and negative pneumatic pressures, iii) shrinks uniformly due to the near zero Poisson's ratio allowing it to preserve intimate contact during activation, and iv) is highly reversible to enable repeated use. The membrane has low adhesion to the foundation, which allows it to separate and inflate for positive pressures. Significantly, the foundation

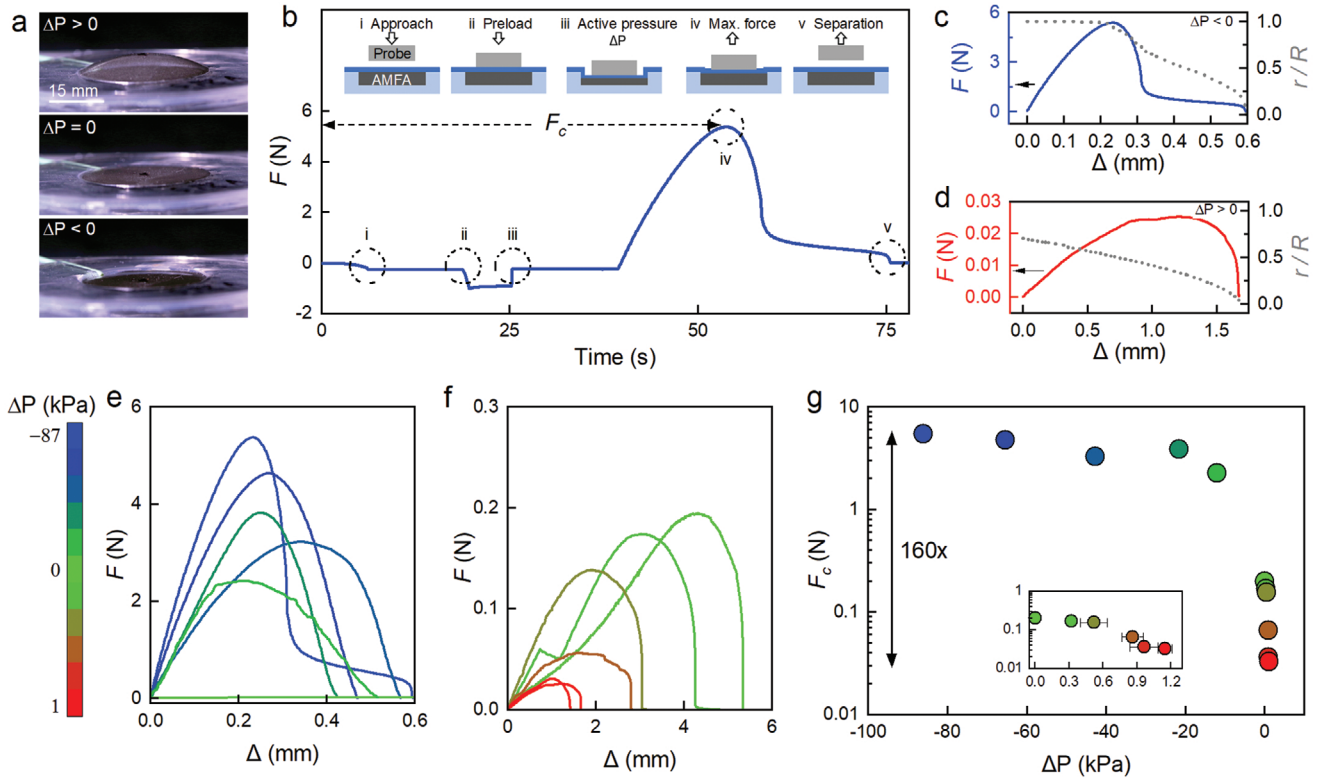

Figure 2. AMFA adhesion characterization. a) Images of the membrane in the positive ($\Delta P > 0$), neutral ($\Delta P = 0$), and negative ($\Delta P < 0$) pneumatic pressure conditions. b) Force (F) as a function of time for a representative adhesion experiment. c,d) (Left y-axis) force (F) versus displacement (Δ) and (right y-axis) contact radius (r) normalized by indenter radius (R) versus Δ for c) $\Delta P = -87$ kPa and d) $\Delta P = 1$ kPa. e) Adhesion F versus Δ curves for $\Delta P < 0$. f) Adhesion F versus Δ curves for $\Delta P > 0$. g) Adhesive force capacity F_c as a function of pneumatic pressure (ΔP), showing an adhesive switching ratio of 160x. The inset shows the data for $\Delta P > 0$. $R = 7.5$ mm, smooth acrylic indenter, $v = 1$ mm min^{-1}, and $t = 100$ µm for all plots.

modulus and thickness are tunable through applied pneumatic pressure, as discussed below. By connecting the adhesive to a pneumatic controller, we can provide positive, neutral, or negative pneumatic pressure to the system (**Figure 2**a). To examine the role of pressure on adhesion, we perform contact adhesion experiments where a flat rigid indenter of radius R is brought into contact with the adhesive, the pneumatic system supplies a pressure, and then the indenter retracts until complete separation occurs. Figure 2b shows a typical normal adhesion curve, where a negative pneumatic pressure shows a dramatic increase in adhesive force capacity (F_c) compared to a positive pneumatic pressure (Figure 2c,d and Video S1, Supporting Information). When examining the contact area during retraction, the negative pressure case stays in near complete contact ($r > 0.9R$ at F_c, where r is contact radius) during retraction until the maximum force is reached, at which point the material begins to separate more rapidly and the contact radius reduces until the force reaches zero (Figure 2c). For the positive pressure case, the contact area begins to shrink during retraction and reduces throughout the retraction phase as seen in Figure 2d. By tuning the negative pneumatic pressure, we find that higher negative pressures result in a higher F_c (Figure 2e), while higher positive pneumatic pressures result in a lower F_c (Figure 2f). By plotting F_c as a function of pressure (ΔP) in Figure 2g, we find an adhesive switching ratio of 160x, demonstrating both a high switching ratio as well as a tunable spectrum of adhesive forces by controlling the pneumatic pressure.

To model the adhesive behavior for negative pressures ($\Delta P < 0$), we consider the foam as a compliant foundation that supports the membrane. When the adhesive stress ($F/\pi R^2$, where R is indenter radius) is larger than the magnitude of the pneumatic pressure, we expect the membrane to lift from the foundation. In this case, the adhesive capacity (F_c) will be proportional to the applied pressure.

$$F_c = -\Delta P \pi R^2 \tag{1}$$

When the adhesive stress is less than the magnitude of the negative pneumatic pressure, the membrane will stay on the foundation. In this case, the behavior is expected to be controlled by the foundation stiffness (E/h). Here, the pneumatic pressure acts as a control for both the foundation thickness ($h(\Delta P)$) as well as its (tangent) modulus ($E(\Delta P)$), which together tune the foundation stiffness.[33] Although (E/h) is sufficient for the analysis, for design insights we choose to maintain foundation modulus and thickness independently in our analysis, as they are both nonlinear functions of applied pressure. One can, for example, maintain a given (E/h) but increase thickness to improve the ability to conform to more complex shapes. In the case where the indenter radius (R) is on the order of, or larger than, the foundation thickness (h), the thickness plays a role in

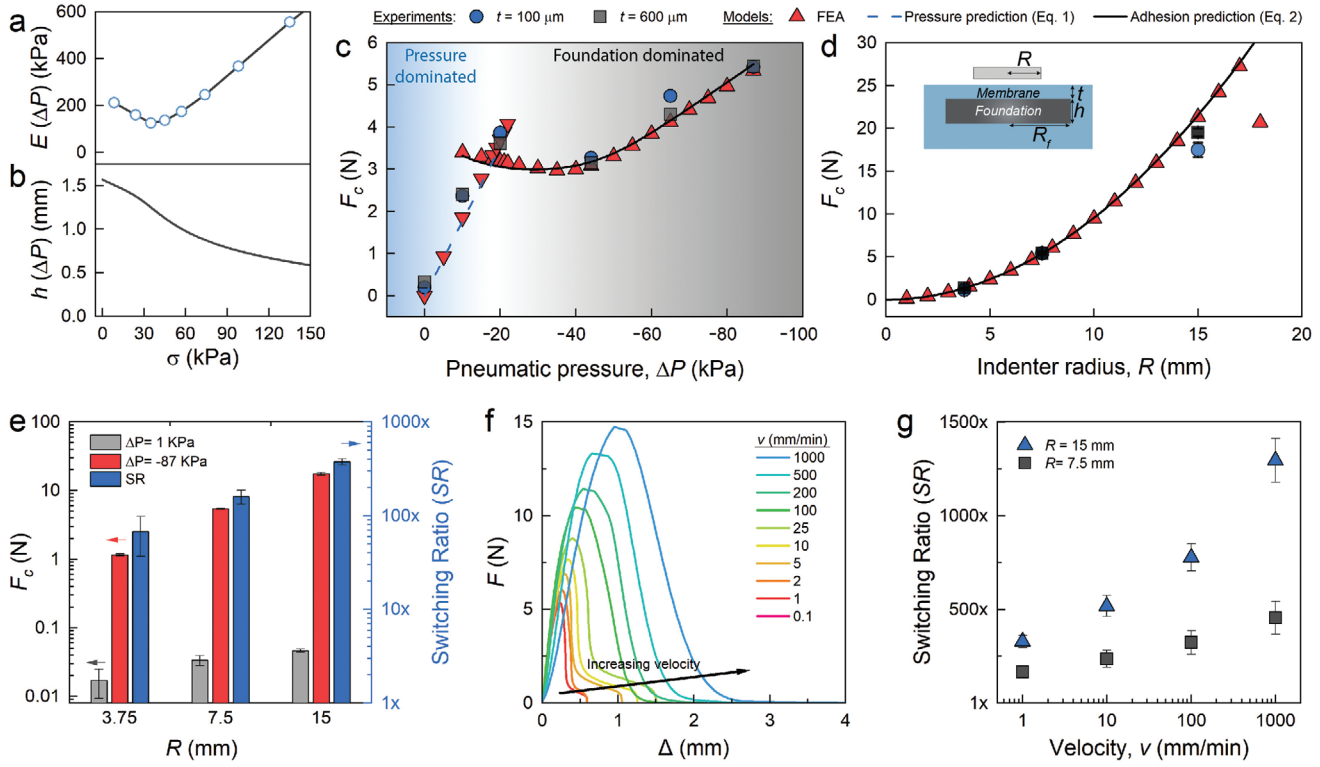

Figure 3. Switchable adhesion and predictions. a) Modulus ($E(\Delta P)$) as a function of pressure and b) foam thickness ($h(\Delta P)$) as a function of pressure. c) Adhesive and FEA data compared to theoretical predictions for $R = 7.5$ mm as a function of pneumatic pressure and d) indenter radius (R) with a constant $\Delta P = -87$ kPa. e) Effect of indenter radius on adhesion for maximum and minimum pneumatic pressure (left y-axis) with the corresponding adhesive switching ratio (right y-axis) for $t = 100$ μm. f) Force (F) versus displacement (Δ) for the $R = 7.5$ mm indenter on $t = 100$ μm membrane for different testing velocities (v). g) Adhesive switching ratio as a function of testing velocity for $t = 100$ μm and different size indenters, showing SR ≈ 1300x for the $R = 15$ mm indenter at $v = 1000$ mm min^{-1}. In component c and d, $G_c = 1.2$ N m^{-1} for all models, $v = 1$ mm min^{-1} unless otherwise noted. All indenters are smooth acrylic.

the adhesion[34–36] and mechanical behavior.[37–40] Therefore, the total energy in the system (U_T) is a summation of the surface energy $U_S = \pi R^2 G_c$, where G_c is the critical strain energy release rate, and the elastic energy $U_E = F^2 h(\Delta P)/2\pi E(\Delta P) R^2$.[34] For a contact area (A), the adhesive capacity is determined when $\partial U_T/\partial A = 0$, where

$$F_c = \left(\frac{2\pi^2 E(\Delta P) G_c R^4}{h(\Delta P)} \right)^{1/2} \quad (2)$$

which shows the dependence of F_c on the applied pneumatic pressure in modulus and thickness. To determine $E(\Delta P)$ and $h(\Delta P)$, we perform uniaxial compression experiments on the foam with a rigid indenter. We observe a nonlinear stress–strain response and measure $E(\Delta P)$ locally along the curve as a function of compressive stress, resulting in a stress-dependent tangent modulus (see Figure S2, Supporting Information for mechanical testing data). As seen in **Figure 3**a,b, the foam shows a typical foam response, where at low strain there is an initial modulus attributed to cell wall bending. As strain increases the material effectively softens as the cell walls buckle, with a minimum modulus near 40 kPa compressive stress, and as strain increases further, the foam densifies and the modulus increases as compressive stress increases.[41] The pressure-dependent foam thickness $h(\Delta P)$ plotted in Figure 3b is calculated as $h = h_0(1 - \varepsilon)$, where h_0 is the initial foam thickness and ε is the strain.

We compare the adhesive predictions to the experimental data for the $t = 100$ μm and $t = 600$ μm membrane thicknesses with $R = 7.5$ mm radius indenter (Figure 3c). For $\Delta P \geq -20$ kPa (i.e., less negative), the adhesive stresses are greater than the pneumatic pressures and are well described by Equation (1). As pneumatic pressure becomes greater than adhesive stress, the membrane stays on the foundation. In this regime, the foundation dominates the adhesive response and we find good agreement with Equation (2) for both film thicknesses without any fitting parameters (G_c is independently measured in Figure S3, Supporting Information). Additionally, F_c does not depend on film thickness for 100 μm ≤ t ≤ 1.1 mm, as seen in Figure S4, Supporting Information, which is expected from the model. We also vary the indenter radius and perform experiments at the maximum negative pneumatic pressure of $\Delta P = -87$ kPa for both film thicknesses (Figure 3d). When we compare these results to Equation (2), we find good agreement, with $F_c \approx R^2$, showing positive scaling with contact area. Results from the finite element analysis (FEA) also show good agreement with the experimental data and analytical models for both ΔP and R. For the numerical F_c predictions presented in Figure 3c,d, $G_c = 1.2$ N m^{-1} as experimentally measured. At the largest

indenter radius (R = 15 mm), we find that the experimental data is lower than the models. We attribute this response to the indenter radius becoming similar to the membrane radius and introducing edge effects. FEA analysis and imaging show that upon the application of negative pneumatic pressure, the membrane is uniformly flat across the majority of the radial coordinate. However, curvature in the membrane begins at $r \approx 15$ mm as shown in Figure S5, Supporting Information, which can initiate detachment for the largest indenter. Overall, for both variable pressure and indenter radius, the force capacity predictions yield good agreement with the experimental data and numerical results. This supports the mechanism of adhesion control through a foundation with pressure-tunable rigidity and thickness and provides design guidelines to precisely control adhesive force.

The influence of probe size on adhesion switching ratio (SR) was also investigated. Figure 3e shows F_c for both the ΔP = −87 kPa and ΔP= 1 kPa as a function of probe size (left y-axis) as well as the switching ratio (right y-axis). It is found that larger probes demonstrated both a greater *Fc* as well as a higher SR, where SR = $67x \pm 30$ and SR = $376x \pm 27$ for R = 3.75 mm and 15 mm, respectively. Further control of adhesion can be obtained by tuning the retraction velocity due to viscoelasticity near the crack tip.[2] Figure 3f shows that for ΔP = −87 kPa, as testing velocity increases, F_c increases. By controlling velocity at the pressure extremes, we then evaluate SR as a function of velocity. Figure 3g presents the switching ratio for two different R values as a function of velocity, where F_{low} is taken at low velocity for ΔP = 1 kPa, and F_{high} is at ΔP = −87 kPa for the given velocity. Here, we find that SR increases with velocity for both indenter sizes, with the largest indenter (R = 15 mm) reaching a switching ratio of $1300x \pm 120$. Furthermore, the adhesive stress at F_c is as high as 85 kPa, which is comparable to vacuum chuck systems. The exceptional switching ratio of AMFAs is enabled by the synergistic mechanisms of active membranes on rigidity tunable foundations and velocity dependent adhesion.

The combination of an adhesive membrane and a compliant foundation with rapidly tunable stiffness opens opportunities to adhere to and grip diverse objects. To demonstrate this utility, we performed picking, holding, and controllable releasing of 10 different irregularly shaped everyday objects, including an array of Skittles candy, a roll of tape, the stud side of a LEGO brick, and a coil of electrical wire (**Figure 4**a–d and Video S2, Supporting Information, all 10 are in Figure S6, Supporting Information). Further, we can manipulate highly porous acrylic discs (>50%) and rough substrates such as frosted glass (see Figure S7, Supporting Information). Manipulation of arrays of elements is also possible. Figure 4e shows a 5 × 5 array of tightly packed 4.75 mm diameter steel spheres being picked up, transported, and then controllably printed on a piece of PDMS (Video S3, Supporting Information). Arrays of LED chips and porous assemblies of metal nuts are also demonstrated (see Figure S8 and Video S4, Supporting Information). This diversity of manipulated objects is challenging with traditional gripping systems (i.e., vacuum and rigid grippers); however, in AMFAs, the combination of an active membrane on a compliant foam foundation, which can conform while passive but can increase adhesion when activated, enables versatility to rapidly pick up and release 2D, 3D, porous, rough, and arrays of objects.

To demonstrate AMFAs as a tool to assemble dissimilar materials, we built a fully functioning soft, stretchable LED device. Here, the circuitry is a flex circuit that was etched and cut into the letters ISU. This material is thin, flexible, and has numerous openings and cuts that would make it difficult to print and handle with traditional gripping tools. Furthermore, we utilize rigid board mount LEDs that turn on when printed due to the presence of eutectic gallium indium (EGaIn) liquid metal on the contacts (Figure 4f and Video S5, Supporting Information). The 20 LEDs are picked up, transported, and then printed onto the circuit from a donor substrate (Figure 4g). Although the LEDs are lightweight (28 mg), they can be released mid-air by the active membrane without a contribution from the underlying substrate, showing the pure adhesion switching effect to release small, lightweight objects (Figure 4h). The device is assembled by the active membrane adhesion by first printing the patterned flex circuit, and then subsequently printing 20 LEDs without any failure (100% printing yield) (Figure 4i). Upon encapsulating the device with PDMS, the device is fully functional and is capable of stretching, bending, and twisting (Figure 4j–l). This demonstration captures the ability to print flat, flexible, porous materials as well as rigid objects with a single device. The programmable rapid attachment and release with excellent yield of AMFAs has the potential to enable material assembly in diverse devices.

AMFAs display rapid adhesive switching with switching ratios as high as $1300x$ with programmable adhesive tunability. This is achieved using the combination of an active membrane to control interfacial shape with a pressure triggered rigidity tunable foam foundation that leverages both positive and negative pneumatic pressures. This allows us to overcome challenges with rigidity tuning and shape changing mechanisms that rely on diffusion (i.e., thermal or fluidic) to enable rapidly switchable adhesion. AMFAs further allow the interface to be compliant during contact formation to maximize contact, yet become rigid when picking up objects to tune adhesive force. This mechanism is supported by analytical and numerical modeling based on the underlying physics of adhesion, which captures how the active control of material stiffness and geometry can tune adhesion behavior to create a spectrum of adhesion values on diverse objects without retooling. Although we primarily focused on a fixed size AMFA, $F_c \approx R^2$, showing adhesion scaling with object contact area. Therefore, AMFAs can be changed in size to accommodate larger or smaller objects as necessary. A PDMS membrane was used throughout our work; however, changing the membrane material could improve compatibility or create specific interactions between the AMFA and the objects to be picked, where the membrane could be tuned for application specific needs. Furthermore, we used a foam foundation actuated through pneumatic pressure, foundations which change stiffness through other stimuli could be combined with the active membrane to tune adhesion. Also, tuning the viscoelasticity of the foundation could potentially provide synergistic effects with the active membrane for pick and place applications. In conclusion, AMFAs create rapid, switchable adhesion on porous, soft, and rigid objects that can

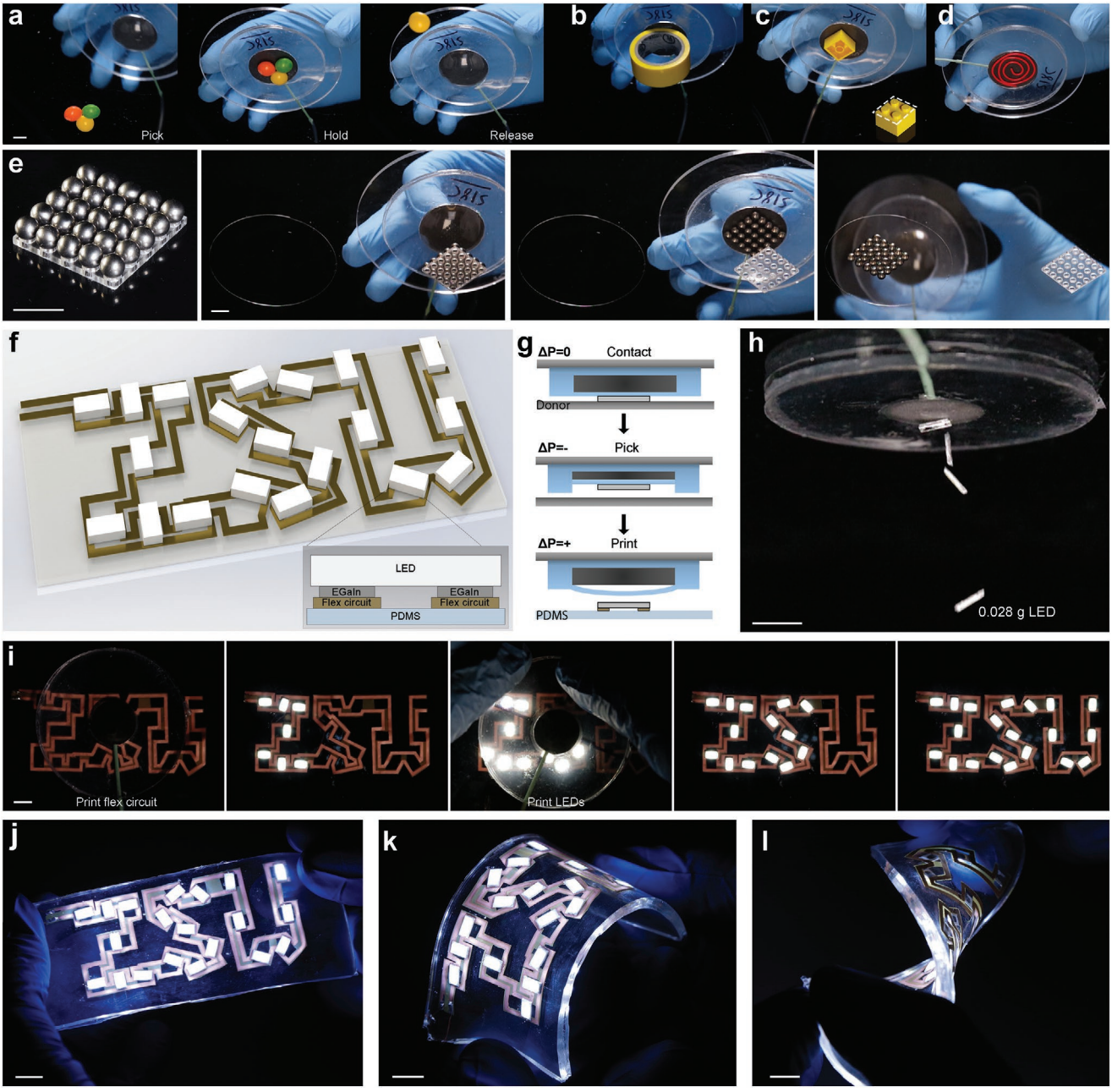

Figure 4. Manipulation of common objects and dissimilar material assembly with AMFAs. a) An array of Skittles candy is picked up, held, and then released from an AMFA. b) This process is repeated for a roll of yellow tape, c) the stud side of a LEGO, and d) a coil of 22 gauge red electrical wire. e) A 5 × 5 array of 4.75 mm diameter steel sphere are picked up off a holder, transported, and then printed onto a PDMS film. f) Schematic of a patterned flex circuit with LEDs to be assembled in the letters ISU; inset shows the LED/circuit configuration. g) Illustration of the the material assembly process. h) Active membrane adhesive releases an 0.028 g LED showing the pure adhesion switching effect in the off state. i) Assembly process with the active membrane that prints a patterned (porous) flex circuit, then prints 20 LEDs in sequence with 100% yield. j) Assembled device encapsulated with PDMS that is k) bent and l) twisted. All scale bars are 10 mm.

be difficult to manipulate with traditional gripping systems. Controlled pick and place manipulations require that adhesion is both high for pick up and low for release. It is therefore important for soft dry adhesives designed for manipulation to not only generate high adhesive forces, but also be able to rapidly switch and generate low adhesive forces to be able to release small or lightweight objects. We show this with AMFAs by manipulating over 20 different types of objects ranging in mass from 0.028 to 400 g (>14 000*x* difference in mass) in both individual and arrayed elements with various surface topographies and porosity/roughness. We anticipate that the materials and mechanisms presented here will be useful in applications such as robotic gripping and locomotion, pick and place operations, and material and device assembly.

Experimental Section

Fabrication: Membranes are made using PDMS (Sylgard 184, Ellsworth Adhesives, 20:1 base:curing agent ratio, cured for 24 h at 80° C) and attached to a cast PDMS body using plasma cleaning (30 s under 0.6 torr oxygen at medium RF level, PDC-001-HP, Harrick Plasma). The treated surfaces were immediately pressed together at room temperature and held together with pressure for at least 12 h. A circular pocket in the body with foundation radius $R_f = 18$ mm was filled with an open-cell foam of nominal 1.57 mm thickness (Poron Very Soft 20 pcf Microcellular Polyurethane, Rogers Corporation). A narrow rigid tube was embedded in the PDMS body from which to control pressure. The top foam surface was sanded with 80 grit sandpaper in order to remove the foam skin.

Testing: AMFAs were tested for normal adhesion behavior on a mechanical testing machine (Instron 5944 load frame). Pads were cleaned with isopropyl alcohol and bottoms were adhered onto a rigid acrylic plate. A circular acrylic probe tip on the end of a mobile sheath was brought into contact with the top membrane at 1 mm min^{-1}. A compressive preload of 5.7 kPa to initially adhere the probe was applied at 5 mm min^{-1}. The position was held for 5 s; positive, negative, or no pressure was applied, and position held for another 5 s. The sheath/probe tip was free to move vertically to accommodate any changes in thickness of the foam upon application of pressure. The tip was then retracted at varying test rates until complete debonding occurred. A mirror system allowed for real-time viewing of the bonding surface (see Figure S9, Supporting Information).

FEA Modeling: Finite element simulations were conducted using ABAQUS/Standard (ABAQUS 2018, Providence, RI) and XSEDE computing resources.[42] The AMFA was modeled as an axisymmetric tri-layer system, as shown in Figure S10, Supporting Information, consisting of lower and upper PDMS layers and a central foam layer, all with radius $R_f = 18$ mm. The thicknesses of the lower and upper PDMS layers were maintained at $b = 1.5$ mm and $t = 0.1$ mm, respectively. The PDMS was defined as a linearly elastic material with Young's modulus $E_s = 800$ kPa and Poisson's ratio $\nu_s = 0.49$. For each applied negative pressure, the foam was idealized as a linearly elastic material with thickness $h = h(\Delta P)$ and Young's modulus $E_f = E_f(\Delta P)$ corresponding to the data from the uniaxial compression experiments (Figure 3a,b), which captured the hyperelastic response of the foam material. The foam was assumed to have a Poisson's ratio $\nu_f = 0$, which is typical for foams at large compressive strains. The effect of an alternative assumption of $\nu_f = 0.3$, which is typical for foams at small strains, was examined as shown in Figure S11, Supporting Information. The simulations were conducted using axisymmetric eight-node hybrid biquadratic elements (CAX8H). With the nodes on the bottom edge of the lower PDMS layer fixed, the nodes on the top edge of the upper PDMS layer along a radial segment R were displaced upward uniformly. For determining F_c, two cases were considered including 1) a pressure applied directly to the bottom edge of the upper PDMS layer and 2) a tie constraint applied at the interface between the upper PDMS and central foam layers without an explicit application of pressure. Both cases are discussed in detail in the Supporting Information. For investigation of the indenter radius effects, the tri-layer system was modified by the extension of the PDMS fs by $R_s = 19.5$ mm, as shown in Figure S10, Supporting Information with results in Figure S12, Supporting Information.

Supporting Information

Supporting Information is available from the Wiley Online Library or from the author.

Acknowledgements

M.D.S. and C.B.H. contributed equally to this work. M.D.S., C.B.H, D.H., and M.D.B. acknowledge support from a 3M Non-Tenured Faculty Award, Iowa State University of Science and Technology, and University Honors Program Stewart Research Award. C.J.S. and K.T.T. acknowledge support from the National Science Foundation NRI under award 1830475. This work used the Extreme Science and Engineering Discovery Environment (XSEDE), which is supported by National Science Foundation grant number ACI-1548562. Specifically, the authors used the Comet cluster provided by the San Diego Supercomputer Center (SDSC) at the University of California San Diego under allocation TG-MSS190018. Poron foam was provided by Rogers Corporation. The authors also acknowledge A.B.M. Haque and R. Tutika for help with surface scans and S. Frey for help with schematics.

Conflict of Interest

The authors declare no conflict of interest.

Keywords

adhesion, gripping, rigidity tuning, soft robotics, switchable adhesion

Received: July 8, 2020
Revised: August 27, 2020
Published online:

[1] A. B. Croll, N. Hosseini, M. D. Bartlett, *Adv. Mater. Technol.* **2019**, *4*, 1900193.
[2] M. A. Meitl, Z. T. Zhu, V. Kumar, K. J. Lee, X. Feng, Y. Y. Huang, I. Adesida, R. G. Nuzzo, J. A. Rogers, *Nat. Mater.* **2006**, *5*, 33.
[3] E. Brown, N. Rodenberg, J. Amend, A. Mozeika, E. Steltz, M. R. Zakin, H. Lipson, H. M. Jaeger, *Proc. Natl. Acad. Sci.* **2010**, *107*, 18809.
[4] S. I. Rich, R. J. Wood, C. Majidi, *Nat. Electron.* **2018**, *1*, 102.
[5] A. Carlson, A. M. Bowen, Y. Huang, R. G. Nuzzo, J. A. Rogers, *Adv. Mater.* **2012**, *24*, 5284.
[6] M. Tatari, A. Mohammadi Nasab, K. T. Turner, W. Shan, *Adv. Mater. Interfaces* **2018**, *5*, 1800321.
[7] J. K. Park, J. D. Eisenhaure, S. Kim, *Adv. Mater. Interfaces* **2019**, *6*, 1801542.
[8] M. Frensemeier, J. S. Kaiser, C. P. Frick, A. S. Schneider, E. Arzt, R. S. FertigIII, E. Kroner, *Adv. Funct. Mater.* **2015**, *25*, 3013.
[9] H. Yi, M. Seong, K. Sun, I. Hwang, K. Lee, C. Cha, T. i. Kim, H. E Jeong, *Adv. Funct. Mater.* **2018**, *28*, 1706498.
[10] W. Wang, J. V. Timonen, A. Carlson, D. M. Drotlef, C. T. Zhang, S. Kolle, A. Grinthal, T. S. Wong, B. Hatton, S. H. Kang, S. Kennedy, J. Chi, R. T. Blough, M. Sitti, L. Mahadevan, J. Aizenberg, *Nature* **2018**, *559*, 77.
[11] R. La Spina, M. Tomlinson, L. Ruiz-P'erez, C. A., S. Langridge, M. Geoghegan, *Angew. Chem. Int. Ed.* **2007**, *46*, 6460.
[12] M. T. Northen, C. Greiner, E. Arzt, K. L. Turner, *Adv. Mater.* **2008**, *20*, 3905.
[13] S. B. Diller, S. H. Collins, C. Majidi, *J. Intell. Mater. Syst. Struct.* **2018**, *29*, 3804.
[14] J. Blass, B. Bozna, M. Albrecht, J. Krings, B. Ravoo, G. Wenz, R. Bennewitz, *Chem. Commun.* **2015**, *51*, 1830.
[15] S. Kim, J. Wu, A. Carlson, S. Jin, A. Kovalsky, P. Glass, Z. Liu, N. Ahmed, S. Elgan, W. Chen, P. Ferreira, M. Sitti, Y. Huang, J. Rogers, *Proc. Natl. Acad. Sci.* **2010**, *107*, 17095.
[16] V. Sariola, M. Sitti, *Adv. Mater. Interfaces* **2014**, *1*, 1300159.
[17] Y. Hao, S. Biswas, E. Hawkes, T. Wang, M. Zhu, L. Wen, Y. Visell, arXiv preprint, arXiv:1912.06753, **2019**.

[18] D. Paretkar, M. Kamperman, D. Martina, J. Zhao, C. Creton, A. Lindner, A. Jagota, R. McMeeking, E. Arzt, *J. R. Soc., Interface* **2013**, *10*, 20130171.
[19] W. G. Bae, D. Kim, K. Y. Suh, *Nanoscale* **2013**, *5*, 11876.
[20] M. D. Bartlett, A. B. Croll, D. R. King, B. M. Paret, D. J. Irschick, A. J. Crosby, *Adv. Mater.* **2012**, *24*, 1078.
[21] J. Krahn, D. Sameoto, C. Menon, *Smart Mater. Struct.* **2011**, *20*, 015014.
[22] E. Chan, J. Karp, R. Langer, *J. Polym. Sci., Part B: Polym. Phys.* **2011**, *49*, 40.
[23] H. Lee, D. S. Um, Y. Lee, S. Lim, H. J. Kim, H. Ko, *Adv. Mater.* **2016**, *28*, 7457.
[24] E. W. Hawkes, E. V. Eason, A. T. Asbeck, M. R. Cutkosky, *IEEE/ASME Trans. Mechatron.* **2013**, *18*, 1.
[25] D. Sameoto, H. Sharif, J. P. D. Téllez, B. Ferguson, C. Menon, *J. Adhes. Sci. Technol.* **2014**, *28*, 354.
[26] D. G. Hwang, K. Trent, M. D. Bartlett, *ACS Appl. Mater. Interfaces* **2018**, *10*, 6747.
[27] A. Carlson, S. Wang, P. Elvikis, P. M. Ferreira, Y. Huang, J. A. Rogers, *Adv. Funct. Mater.* **2012**, *22*, 4476.
[28] S. Song, M. Sitti, *Adv. Mater.* **2014**, *26*, 4901.
[29] H. Luo, C. Wang, C. Linghu, K. Yu, C. Wang, J. Song, *Natl. Sci. Rev.* **2020**, *7*, 296.
[30] C. Linghu, C. Wang, N. Cen, J. Wu, Z. Lai, J. Song, *Soft Matter* **2019**, *15*, 30.
[31] S. Song, D. M. Drotlef, C. Majidi, M. Sitti, *Proc. Natl. Acad. Sci.* **2017**, *114*, E4344.
[32] P. Glick, S. A. Suresh, D. Ruffatto, M. Cutkosky, M. T. Tolley, A. Parness, *IEEE Robot. Autom. Lett.* **2018**, *3*, 903.
[33] D. A. Dillard, B. Mukherjee, P. Karnal, R. C. Batra, J. Frechette, *Soft Matter* **2018**, *14*, 3669.
[34] K. Kendall, *J. Phys. D: Appl. Phys.* **1971**, *4*, 1186.
[35] J. Ganghoffer, A. Gent, *J. Adhes.* **1995**, *48*, 75.
[36] J. Nase, O. Ramos, C. Creton, A. Lindner, *Eur. Phys. J. E* **2013**, *36*, 103.
[37] J. Menčík, D. Munz, E. Quandt, E. Weppelmann, M. Swain, *J. Mater. Res.* **1997**, *12*, 2475.
[38] R. Saha, W. D. Nix, *Acta Mater.* **2002**, *50*, 23.
[39] H. Li, J. J. Vlassak, *J. Mater. Res.* **2009**, *24*, 1114.
[40] Y. Zhang, Y. p. Zhao, Z. Cheng, *J. Phys. D: Appl. Phys.* **2018**, *51*, 065305.
[41] L. J. Gibson, M. F. Ashby, *Cellular Solids: Structure and Properties*, Cambridge University Press, Cambridge, UK **1999**.
[42] J. Towns, T. Cockerill, M. Dahan, I. Foster, K. Gaither, A. Grimshaw, V. Hazlewood, S. Lathrop, D. Lifka, G. D. Peterson, R. Roskies, J. R. Scott, N. Wilkins-Diehr, *Comput. Sci. Eng.* **2014**, *16*, 62.